Numerical State-Space Average-Value Modeling of PWM DC-DC Converters Operating in DCM and CCM

Ali Davoudi, *Student Member, IEEE*, Juri Jatskevich, *Member, IEEE*, and Tom De Rybel

***Abstract*—State-space average-value modeling of pulsewidth modulation converters in continuous and discontinuous modes has received significant attention in the literature, and various models have been developed. This paper presents a new approach for generating the state-space average-value model. In the proposed methodology, the so-called duty-ratio constraint and the correction term are extracted numerically using the detailed simulation and are expressed as nonlinear functions of the duty cycle and average-value of the fast state variable. The parasitic effects of circuit elements are readily included. The resulting average-value model is compared to a hardware prototype, a detailed simulation, and several previously published models. The proposed model is shown to be very accurate in predicting the large-signal time-domain transients as well as the small-signal frequency-domain characteristics.**

***Index Terms*—Average-value modeling, dc–dc converters, discontinuous conduction mode (DCM), state-space averaging.**

I. Introduction

ACCURATE models of dc–dc converters are often required. The detailed models, wherein the switching of each power-electronic device is represented, can be readily built and implemented using various commercially available simulation software packages and toolboxes. However, the so-called average-value models, wherein the effects of fast switching are neglected or "averaged" with respect to the prototypical switching interval, are frequently required when investigating power-electronic-based systems [1]–[3]. The continuous large-signal (transient) models are typically nonlinear and can be linearized around a desired operating point. Many simulation programs offer automatic linearization and subsequent state-space and/or frequency-domain analysis tools [4], [5]. Thereafter, obtaining a local transfer-function becomes a straightforward and virtually instantaneous procedure. It has been shown in [6] that the asymptotical stability of the average-value model and that of a detailed switching circuit are equivalent. Therefore, the calculated transfer-functions may be used to design the controllers. Additionally, the average-value models typically execute orders of magnitude faster than the corresponding detailed simulations, making them ideal for representing the respective components in system-level studies.

Many averaging methods are based on a specific ideal topology and piecewise linear (triangular) waveform of the current and/or voltage. A similar approach to averaging, the so-called sampled-data modeling, takes into account the time-variant discrete nature of the converters [7]–[10]. This approach looks at the cycle-by-cycle behavior and suppresses the internal details within a switching cycle [11]. However, since the basic sampled-data models neglect the dynamics of state variables in between the sample instances, inaccuracy arises in predicting high-frequency dynamics [12], [13]. Average-value modeling is also often performed by averaging the switching network and/or it elements. This approach is known as circuit averaging or averaged-switch modeling [14]–[17]. In this and similar approaches [18]–[20], the switching elements in a switch-cell are replaced with the appropriate controlled sources. Another systematic approach, often referred to as state-space averaging, involves manipulation of the state-space equations (matrices) of the converter system. The analytical derivation of this method is based on a given operation mode, such as continuous or discontinuous, and on a small-ripple approximation [21], [22].

Although considering ideal/lossless components significantly simplifies the model development, neglecting the parasitic effects in averaged models may sometimes lead to failure in predicting the fast-scale instabilities [23]. Parasitics are also considered in the design stage when the performance, efficiency, and robustness of a system are considered [24]. Parasitics are often modeled as appropriate equivalent series resistances (ESR) associated with the circuit components. However, if losses due to the switch and/or inductor are taken into account, the analytical derivations become more challenging. Steady-state and small-signal analysis of switching converters with parasitics have been studied in [25]–[27]. A large-signal averaged model can be found in [28], which considers some but not all parasitics. The analytical derivation also becomes more complicated when the number of energy storage elements is increased [29] and/or the fast state variable is held at a nonzero constant value within the discontinuous subinterval [30].

In this paper, a new method of constructing average-value models is presented. The properties of the proposed model and the contributions of this paper can be summarized as follows.

- First, it is shown how the conventional state-space averaged equation can be corrected to include the fast dynamics of the discontinuous state variables.

Manuscript received May 24, 2005; revised November 11, 2005. Recommended by Associate Editor M. Ferdowsi.

A. Davoudi is with the University of Illinois at Urbana-Champaign, Urbana, IL 61820 USA.

J. Jatskevich and T. De Rybel are with the Department of Electrical and Computer Engineering, University of British Columbia, Vancouver, BC V6T 1Z4 Canada (e-mail: jurij@ece.ubc.ca).

Digital Object Identifier 10.1109/TPEL.2006.876848

- Unlike many previously derived models, the proposed model is numerically constructed using the corrected state-space formulation and the detailed model of the converter under study.
- The proposed model can be used in continuous and discontinuous modes without special consideration for the boundary mode or the transition between modes.
- The proposed methodology is demonstrated on a boost converter and can be applied to other topologies. Moreover, the model has a well-defined structure that provides the framework for further automating the approach.
- The resulting averaged model is non-linear, explicit, continuous, and valid for large-signal transients as well as for linearization and small-signal characterization.
- Any parasitics present in the detailed model are automatically included in the final averaged model without requiring extensive analytical derivations.
- The proposed model has been compared with the most up-to-date published state-space averaged model [31], as well as several other previously published models [16], [17], [28], [32], [33].
- The accuracy of the generated average-value model has been verified in time-domain as well as frequency-domain against the hardware prototype, the detailed simulation, and several conventional analytically-derived average-value models.

II. General Framework

Switched converters are often modeled as piece-wise linear networks in which the topology changes at the boundaries between subsequent subintervals within a prototypical switching cycle [34]. Based on the state of each switching element, such as transistor and diode, the appropriate state-space equations can be derived [35]. The state variables are typically associated with the energy storage components. In addition, there are well-defined algorithms [36] and software tools [37]–[41] that automatically generate and dynamically update the state-space model for each new topological state of the system being studied. Regardless of the approach or tool used, it is assumed that inside each k-th subinterval the system state model may be expressed by the system matrices $\mathbf{A}_k, \mathbf{B}_k, \mathbf{C}_k$, and $\mathbf{D}_k$.

As a representative of basic topologies, a boost converter circuit shown in Fig. 1(a) is considered in this paper. The inductor current and capacitor voltage define the state vector $\mathbf{x} = [i_L, v_c]^T$. The converter switching frequency is denoted by f_s and a prototypical switching interval is $T_s = 1/f_s$. In comparison to the fast dynamic response of the inductor current, the capacitor voltage typically undergoes slower dynamic transient and usually remains continuous. Thus, in the given topology, the inductor current and capacitor voltage may be called the fast and slow state variables, respectively. In continuous conduction mode (CCM), switching interval T_s is divided into two subintervals $(k = 1,2), (t_0, t_1)$ and (t_1, t_2), and the respective duty cycles are d_1 and $d_2 = 1 - d_1$. It is assumed that the active switch duty cycle d_1 is controlled externally.

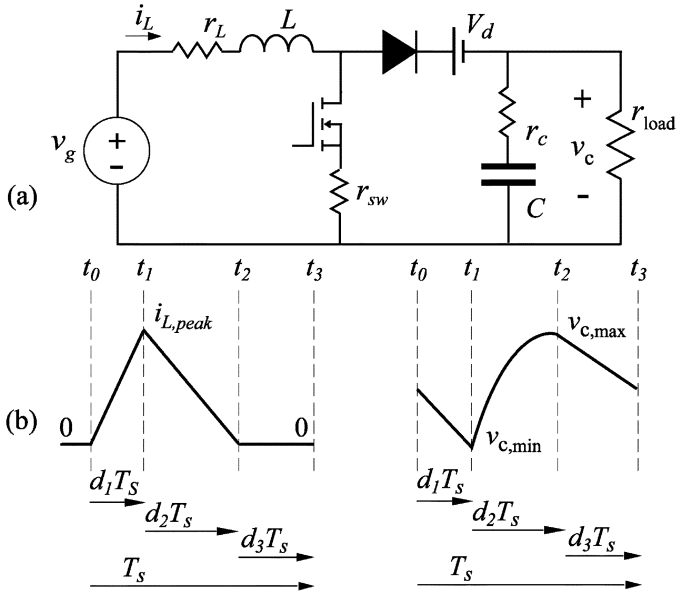

Fig. 1. (a) Boost converter circuit diagram and (b) idealized state variable waveforms for a lossless converter in DCM.

The state-space averaging of CCM has been presented previously in numerous publications [21], [42], [43], and ([44], Chap. 7). The converter's state-space equation in this mode is

$$\dot{\mathbf{x}}(t) = (q(t)\mathbf{A}_1 + (1 - q(t))\mathbf{A}_2)\mathbf{x}(t) + (q(t)\mathbf{B}_1 + (1 - q(t))\mathbf{B}_2)\mathbf{u}(t) \quad (1)$$

where $q(t)$ is the switching function, $\mathbf{A}_k, \mathbf{B}_k$ are the system matrices, and $\mathbf{u}(t)$ is an input vector. By definition, the so-called fast average of a state variable $x(t)$ over a prototypical switching interval is

$$\bar{x}(t) = \frac{1}{T_s}\int_{t-T_s}^{t} x(\tau)d\tau. \quad (2)$$

The resulting $\bar{x}(t)$ is also called the actual or the true average of $x(t)$. Since the averaging is commutative with respect to differentiation, taking the fast average of (1) over a prototypical switching interval yields

$$\dot{\bar{\mathbf{x}}}(t) = (d(t)\mathbf{A}_1 + (1 - d(t))\mathbf{A}_2)\bar{\mathbf{x}}(t) + (d(t)\mathbf{B}_1 + (1 - d(t))\mathbf{B}_2)\mathbf{u}(t). \quad (3)$$

This result follows from the fact that the fast average of the switching function over a prototypical switching interval is the duty cycle function

$$d(t) = \frac{1}{T_s}\int_{t-T_s}^{t} q(\tau)d\tau. \quad (4)$$

It is also assumed that the average of the product is equal to the product of the averages, especially

$$\overline{\mathbf{Bu}} = \bar{\mathbf{B}} \cdot \bar{\mathbf{u}} \quad (5)$$

$$\overline{\mathbf{Ax}} = \bar{\mathbf{A}} \cdot \bar{\mathbf{x}}. \quad (6)$$

TABLE I
CONVENTIONAL AVERAGE-VALUE MODELS FOR A BOOST CONVERTER OPERATING IN DCM

Averaged model	Averaged state-space equations	Low-frequency pole	High-frequency pole	RHP zero
Reduced-order models [31],[32],[43]	$\frac{d\bar{v}_c}{dt}=\frac{v_{in}^2}{2LC}\cdot\frac{d_1^2T_s}{\bar{v}_c-v_{in}}-\frac{\bar{v}_c}{RC}$	$\frac{2\frac{V_c}{V_g}-1}{(\frac{V_c}{V_g}-1)RC}$	None	None
Full-order models [17],[33],[44]	$\frac{d\bar{i}_L}{dt}=\frac{v_{in}}{L}-\frac{2\bar{i}_L\bar{v}_c}{d_1^2T_s\bar{v}_c+2L\bar{i}_L}$ $\frac{d\bar{v}_c}{dt}=\frac{2L\bar{i}_L^2}{C(d_1^2T_s\bar{v}_c+2L\bar{i}_L)}-\frac{\bar{v}_c}{RC}$	$\frac{2\frac{V_c}{V_g}-1}{(\frac{V_c}{V_g}-1)RC}$	$\frac{2(\frac{V_c}{V_g}-1)^2f_s}{d_1^2(\frac{V_c}{V_g})^2}$	$\frac{2(\frac{V_c}{V_g}-1)f_s}{d_1^2(\frac{V_c}{V_g})}$
Corrected full-order models [28],[31],[48]	$\frac{d\bar{i}_L}{dt}=\frac{2\bar{i}_L}{d_1T_s}(1-\frac{\bar{v}_c}{v_g})+\frac{d_1\bar{v}_c}{L}$ $\frac{d\bar{v}_c}{dt}=\frac{\bar{i}_L}{C}-\frac{{d_1}^2T_sv_g}{2LC}-\frac{\bar{v}_c}{RC}$	$\frac{2\frac{V_c}{V_g}-1}{(\frac{V_c}{V_g}-1)RC}$	$\frac{2(\frac{V_c}{V_g}-1)f_s}{d_1}$	$\frac{2f_s}{d_1}$

Assumption (5) is usually accepted when the source ripple is neglected. Assumption (6) is acceptable if the original switching variables do not deviate significantly from their average values (small ripple approximation) and system matrices $\mathbf{A}_1$ and $\mathbf{A}_2$ commute [22]. These two assumptions are commonly used for converters working in CCM [21] and have been applied to the boundary mode case [45].

In discontinuous conduction mode (DCM), there are three topological states ($k = 1,2,3$). In this mode, a prototypical switching interval is divided into three subintervals corresponding to d_1, d_2, and $d_3 = 1 - d_1 - d_2$, respectively. The inductor current i_L and the capacitor voltage v_c in this mode are shown in Fig. 1(b) for a lossless boost converter, wherein i_L goes to zero when both switch and diode are off. Conventional state-space averaging for converters working in DCM has been summarized in [31], [32], ([44], Chap. 7), and ([46], Chap. 6). For this mode, the direct extension of (1)–(3) results in

$$\dot{\bar{\mathbf{x}}}(t)=(d_1\mathbf{A}_1+d_2\mathbf{A}_2+d_3\mathbf{A}_3)\bar{\mathbf{x}}(t)+(d_1\mathbf{B}_1+d_2\mathbf{B}_2+d_3\mathbf{B}_3)\mathbf{u}(t) \quad (7)$$

which is no longer accurate. The conventional state-space averaging method in (7) averages only the system matrices and not necessarily the state variables themselves [31]. The simplifying assumption made in (6) now presents a problem for the fast state variable i_L, which is zero in the third subinterval. In particular, the local average of i_L in the third subinterval (t_2, t_3) is zero [see Fig. 1(b)], whereas the conventional state-space averaging implies that this value should be $d_3\bar{i}_L$. Since $\bar{i}_L$ is not zero, the result of the conventional state-space averaging is not zero unless the length of the discontinuous subinterval d_3 is zero, which is only true in CCM. The reader may also find an excellent discussion in [31] describing the inconsistency of (7) in terms of predicting the capacitor charging current. Moreover, d_2 becomes a dependent variable that can now be expressed as an algebraic function of other system variables. This dependency of d_2 is frequently called the duty-ratio constraint [31], ([44] Ch. 11).

III. ANALYTICAL DERIVATION AND THE MODEL ORDER

In second-order dc-dc converters (i.e., boost, buck, and buck-boost) operating in DCM, the transfer-functions exhibit dominant low-frequency pole and zero due to the slow state variable dynamics. The pole and the possible right-half-plane zero due to fast state variable dynamics typically occur in higher frequencies, near or exceeding switching frequency. To provide an accurate average-value model via state-space averaging, the duty-ratio constraint has been found to be the key distinction between the reduced-order, full-order, and corrected full-order models [13]. Although these models can be provided through either the state-space averaging or the circuit averaging, the resulting system equations are often identical and/or equivalent. For consistency, the representative models are summarized in Table I, wherein the location of both low and high frequency poles and zeros are shown. As seen in the corrected full-order model, the second pole is located at $(2(V_c/V_g-1)f_s/d_1)$, which can easily exceed the switching frequency. Also, right-hand-plane zero is located at frequency $(2f_s/d_1)$, which is more than twice the switching frequency. This fact often justifies the use of reduced-order models that neglect fast dynamics.

A. Reduced-Order Model

The fast dynamics of i_L in DCM can sometimes be neglected when considering responses in the range of lower frequencies. In this case, the average-value of i_L can be expressed as an algebraic function of the remaining variables. Also, d_2 can be expressed as a function of the control signal d_1 and the average-value of the slow state variable $\bar{v}_c$ (state-space averaging [32], circuit averaging [16]). A principle of volt-second balance that implies a steady-state inductor current waveform ([44],

pp. 20–24), ([46], pp. 13–14) is often utilized. A symbolic analysis program based on the volt-second balance has been introduced to generate the reduced-order averaged models [42], [43]. The resulting models accurately predict the low-frequency response up to roughly one-tenth of the switching frequency [13], [31], [47]. However, at higher frequencies, errors become very noticeable especially in the phase plot.

B. Full-Order Model

The inductor current dynamics are included in the full-order average-value models (equivalent duty ratio [33], loss-free resistor ([44], Ch. 11), and averaged-switch model [17]), which show great improvement over the reduced-order models. Also, some effort is undertaken in [49] to include conduction losses based on the switch-cell introduced in [17]. However, the resulting full-order models are still based on volt-second balance over the inductor, while the presence of inductor dynamics within the switching interval implies that the voltage over the inductor may differ from zero. The reader may find a good discussion of this averaging paradox in [50], which shows that the averaging over one switching cycle can be viewed as a sampling of the true averaging. It was concluded in [13] and [50] that the volt-second balance may result in a modeling error due to violation of the Nyquist sampling theorem. The resulting high-frequency pole and right-hand-plane zero are therefore not predicted accurately. Consequently the phase-lag and the magnitude-drop caused by the inductor dynamics are overestimated [13], [31].

C. Corrected Full-Order Model

More recently, corrected full-order averaged models that very accurately capture the high-frequency dynamics of inductor current i_L were proposed for circuit averaging [48] and state-space averaging [31]. Volt-second balance was not used in these models; instead, d_2 is expressed as a function of the control signal d_1 and the average-value of the fast state $\overline{i}_L$. Using the new representation of d_2 and correcting the state-space model (7) with the special correction matrix [31], a corrected full-order model for ideal dc-dc converters can be obtained. Including the losses for improving the model accuracy is not a trivial task often requiring laborious derivations that are model/topology-specific. Moreover, not all types of parasitics are easily included in all of the models. Some parasitics have been considered in [28] using the switch-cell established in [48].

IV. Numerical Average-Value Modeling

A. Correction Term

The methodology proposed in this paper is based on state-space averaging [31] and assumes a non-ideal converter circuit. In particular, to obtain a correct state-space averaged equation for DCM, one should consider true averaging from the very beginning. In the following discussion, it is instructive to partition the state vector $\mathbf{x}$ within the prototypical switching interval T_s as $\mathbf{x} = \mathbf{x}_1 + \mathbf{x}_2 + \mathbf{x}_3$ corresponding to each subinterval shown in Fig. 1(b). In particular

$$\mathbf{x}_1(t) = \begin{cases} \mathbf{x}(t), & 0 \le t < d_1 T_s \\ 0, & \text{elsewhere} \end{cases} \tag{8}$$

$$\mathbf{x}_2(t) = \begin{cases} \mathbf{x}(t), & d_1 T \le t < (d_1 + d_2) T_s \\ 0, & \text{elsewhere} \end{cases} \tag{9}$$

$$\mathbf{x}_3(t) = \begin{cases} \mathbf{x}(t), & (d_1 + d_2) T_s \le t < T_s \\ 0, & \text{elsewhere.} \end{cases} \tag{10}$$

The corresponding state models are

$$\dot{\mathbf{x}}_1(t) = \begin{cases} \dot{\mathbf{x}}(t) = \mathbf{A}_1 \mathbf{x}(t) + \mathbf{B}_1 \mathbf{u}, & 0 < t < d_1 T_s \\ 0, & \text{elsewhere} \end{cases} \tag{11}$$

$$\dot{\mathbf{x}}_2(t) = \begin{cases} \dot{\mathbf{x}}(t) = \mathbf{A}_2 \mathbf{x}(t) + \mathbf{B}_2 \mathbf{u}, & d_1 T_s < t < (d_1 + d_2) T_s \\ 0, & \text{elsewhere} \end{cases} \tag{12}$$

$$\dot{\mathbf{x}}_3(t) = \begin{cases} \dot{\mathbf{x}}(t) = \mathbf{A}_3 \mathbf{x}(t) + \mathbf{B}_3 \mathbf{u}, & (d_1 + d_2) T_s < t < T_s \\ 0, & \text{elsewhere.} \end{cases} \tag{13}$$

Taking the formal average of (11)–(13) produces the local average models. In particular, the local average of the first subinterval (11) implies

$$\dot{\bar{\mathbf{x}}}_1 = \frac{1}{T_s} \int_0^{d_1 T_s} (\mathbf{A}_1 \mathbf{x}(\tau) + \mathbf{B}_1 \mathbf{u}) d\tau \tag{14}$$

Since $\mathbf{A}_1$ and $\mathbf{B}_1\mathbf{u}$ terms are constant, and

$$\frac{1}{T_s} \int_0^{d_1 T_s} \mathbf{x}(\tau)\, d\tau = \frac{1}{T_s} \int_0^{T_s} \mathbf{x}_1(\tau)\, d\tau = \bar{\mathbf{x}}_1, \tag{15}$$

we get

$$\dot{\bar{\mathbf{x}}}_1 = \mathbf{A}_1 \bar{\mathbf{x}}_1 + d_1 \mathbf{B}_1 \mathbf{u}. \tag{16}$$

Applying the same procedure to (12) and (13) results in

$$\begin{cases} \dot{\bar{\mathbf{x}}}_1 = \mathbf{A}_1 \bar{\mathbf{x}}_1 + d_1 \mathbf{B}_1 \mathbf{u} \\ \dot{\bar{\mathbf{x}}}_2 = \mathbf{A}_2 \bar{\mathbf{x}}_2 + d_2 \mathbf{B}_2 \mathbf{u} \\ \dot{\bar{\mathbf{x}}}_3 = \mathbf{A}_3 \bar{\mathbf{x}}_3 + d_3 \mathbf{B}_3 \mathbf{u} \end{cases}. \tag{17}$$

The final averaged system-equation is obtained from (17) as

$$\dot{\bar{\mathbf{x}}} = \dot{\bar{\mathbf{x}}}_1 + \dot{\bar{\mathbf{x}}}_2 + \dot{\bar{\mathbf{x}}}_3 = (\mathbf{A}_1 \bar{\mathbf{x}}_1 + \mathbf{A}_2 \bar{\mathbf{x}}_2 + \mathbf{A}_3 \bar{\mathbf{x}}_3) + (d_1 \mathbf{B}_1 + d_2 \mathbf{B}_2 + d_3 \mathbf{B}_3)\mathbf{u}. \tag{18}$$

Equation (18) can be rewritten as

$$\dot{\bar{\mathbf{x}}} = (d_1 \mathbf{A}_1 \mathbf{W}_1 + d_2 \mathbf{A}_2 \mathbf{W}_2 + d_3 \mathbf{A}_3 \mathbf{W}_3)\bar{\mathbf{x}} + (d_1 \mathbf{B}_1 + d_2 \mathbf{B}_2 + d_3 \mathbf{B}_3)\mathbf{u} \tag{19}$$

where the diagonal weighting-correction matrix is $\mathbf{W}_k = \mathrm{diag}[\omega_{1k}, \omega_{2k}]$ with the entries defined as

$$\omega_{1,k} = \frac{\bar{i}_{L,k}}{d_k \bar{i}_L} \quad \text{and} \quad \omega_{2,k} = \frac{\bar{v}_{c,k}}{d_k \bar{v}_c}. \tag{20}$$

Here, since the actual average of i_L in the third subinterval is zero, the correction coefficient ω_{13} is zero as defined by (20). Finally, through an observation of (7) and (19), a correction matrix can be defined as

$$\mathbf{M} = \left[\sum_{k=1}^{3} d_k \mathbf{A}_k\right]^{-1} \cdot \left[\sum_{k=1}^{3} d_k \mathbf{A}_k \mathbf{W}_k\right] \tag{21}$$

whereas the corrected state-space averaged equation can be expressed as

$$\dot{\bar{\mathbf{x}}}(t) = (d_1\mathbf{A}_1 + d_2\mathbf{A}_2 + d_3\mathbf{A}_3)\mathbf{M}\bar{\mathbf{x}}(t) + (d_1\mathbf{B}_1 + d_2\mathbf{B}_2 + d_3\mathbf{B}_3)\mathbf{u}(t). \tag{22}$$

This result is similar to the analytical derivation in [31], where $\mathbf{M}$ is also a diagonal matrix. In particular, for the lossless circuit considered in [31], the inductor current i_L has a triangular waveform [Fig. 1(b)], and the diagonal entries corresponding to i_L and v_c have been found to be $(1/(d_1 + d_2))$ and 1, respectively. It is important to note that because the derivative of the discontinuous state i_L in the third subinterval is zero, the corresponding entries of $\mathbf{A}_3$ and $\mathbf{B}_3$ have zeros too. Therefore, the correction coefficient ω_{13} could be any non-zero value that would multiply with the corresponding column of $\mathbf{A}_3$ to zero and give the correct final result. Moreover, if the other two correction coefficients for the inductor current, ω_{11} and ω_{12}, are assumed to be equal, which holds if and only if

$$\frac{\bar{\mathbf{x}}_1(1)}{d_1} = \frac{\bar{\mathbf{x}}_2(1)}{d_2} \tag{23}$$

then, ω_{13} can be set to be

$$\omega_{13} = \omega_{11} = \omega_{12}. \tag{24}$$

So, if one assumes a triangular waveform of i_L and the condition (24), it can be readily verified that the correction matrix $\mathbf{M}$, as defined by (21), will come out diagonal with the entries exactly as those in [31]. However, the inductor losses and capacitor dynamics are neglected by assuming a triangular waveform of i_L. When the parasitics are included, the correction coefficients (20) for the inductor current are not equal. Moreover, including the parasitics of the circuit's components will violate (23) and (24). Consequently, the correction matrix $\mathbf{M}$ will not diagonal. The advantage of having a diagonal correction matrix is that each averaged-state variable has its own correction weight decoupled from the other states. Therefore, a modified correction matrix $\mathbf{M}_\Delta$ should be defined, which can be made diagonal by construction, assuming $\bar{\mathbf{x}}(j) \neq 0$ for $j = 1,2$. Specifically

$$\mathbf{M}\bar{\mathbf{x}} = \mathbf{M}_\Delta \bar{\mathbf{x}} = \mathbf{p} \tag{25}$$

and

$$m_j = \mathbf{M}_\Delta(j,j) = \frac{\mathbf{p}(j)}{\bar{\mathbf{x}}(j)} \tag{26}$$

where $\mathbf{M}_\Delta$ is diagonal with entries m_j. Thereafter, $\mathbf{M}_\Delta$ is used in the corrected state-space averaged (22). Also, since the slow state variable v_c complies with the small ripple approximation, the entry of $\mathbf{M}_\Delta$ corresponding to the slow state variable is usually 1. In the case of higher-order converters, the correction matrix can be partitioned into a diagonal matrix for the discontinuous state variables and an identity matrix for the continuous ones.

B. Model Implementation

The detailed switching model (which includes all the necessary parasitics) should be constructed first. If a state-variable approach is used to implement the detailed simulation, the system matrices $\mathbf{A}_k, \mathbf{B}_k, \mathbf{C}_k$, and $\mathbf{D}_k$ in each subinterval can be extracted numerically. Using the detailed simulation, it is easier to extract the correction matrix $\mathbf{M}_\Delta$, rather than extracting the weighting correction matrices $\mathbf{W}_k$ in each subinterval. Herein, without loss of generality, we assume that there is only one control input d_1 and one discontinuous conduction subinterval d_3. However, the methodology can be extended to converters with more complex topologies [29], [51]–[53]. In the proposed framework, the diagonal elements of the correction matrix $\mathbf{M}_\Delta$ and the duty-ratio constraint d_2 are obtained as functions of the duty cycle d_1 and the average-value of the fast state variable $\bar{i}_L$, which ensures a full-order of the resulting model. To obtain the values of $d_2(d_1, \bar{i}_L)$ and $\mathbf{M}_\Delta(d_1, \bar{i}_L)$, the detailed model is run in the operating region of interest, whereas the state variables are averaged numerically over the prototypical switching interval. In particular, the average-value of the state vector $\bar{\mathbf{x}}$ is computed in a steady state corresponding to a given operating point. Specifically, in the steady-state we have

$$0 = \left(\sum_{k=1}^{3} d_k \mathbf{A}_k\right) \mathbf{M}_\Delta \bar{\mathbf{x}} + \left(\sum_{k=1}^{3} d_k \mathbf{B}_k\right) \mathbf{u} \tag{27}$$

from which the vector $\mathbf{p}$ is computed as

$$\mathbf{p} = -\left[\sum_{k=1}^{3} d_k \mathbf{A}_k\right]^{-1} \cdot \left[\sum_{k=1}^{3} d_k \mathbf{B}_k \mathbf{u}\right]. \tag{28}$$

Thereafter, the diagonal entries of $\mathbf{M}_\Delta$ are found using the computed $\mathbf{p}$ and $\bar{\mathbf{x}}$ according to (26). To obtain the functions $\mathbf{M}_\Delta(d_1, \bar{i}_L)$ and $d_2(d_1, \bar{i}_L)$ for the desired operating range, the detailed simulation is run with different values of the control variable d_1 as well as the load r_{load}. The variables resulting from this procedure are $d_1, d_2, d_3, \bar{i}_L$, and $\bar{v}_c$, and the correction matrix is computed using (26)–(28). These variables are stored for future use in lookup tables, wherein an interpolation/extrapolation may be used as necessary.

It should be pointed out that the numerical robustness of (21) and (28), and therefore of the proposed procedure, depends on the condition number of $\sum_{k=1}^{3} d_k \mathbf{A}_k$. Specifically, if the condition number is very high, implying that the matrix is close

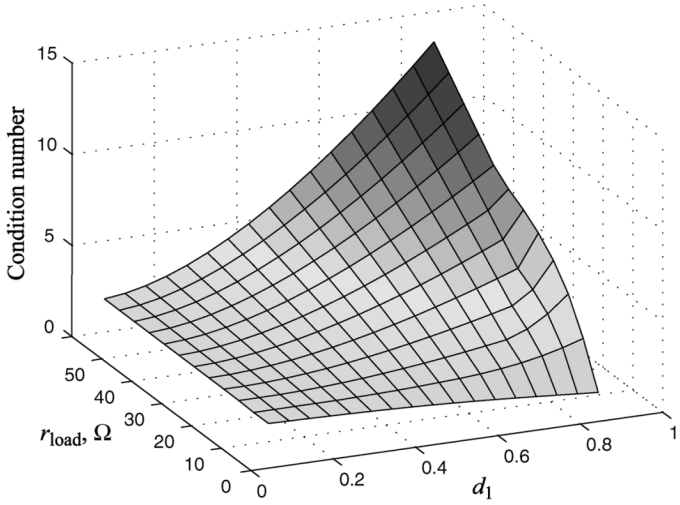

Fig. 2. Condition number of the left multiplier in (21) and (28) for the considered operating range.

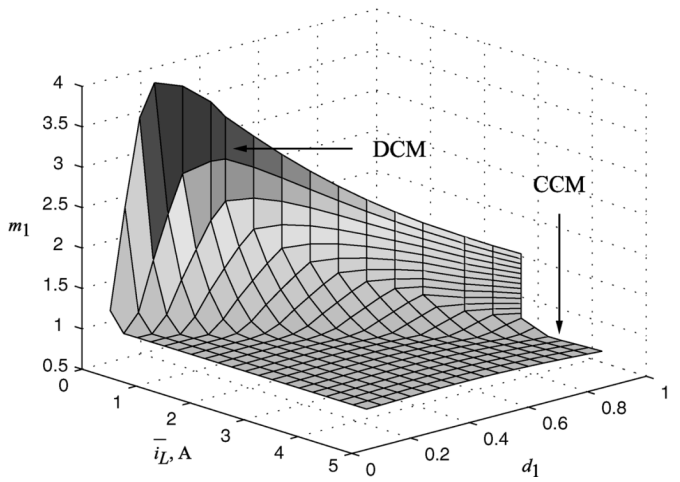

Fig. 3. Fast state variable composite correction coefficient m_1.

to being singular, significant numerical errors may occur [54]. However, the interested reader may consider matrices $\mathbf{A}_k$ found in [31] and observe that since $\mathbf{A}_2$ always has a full rank and $d_2 > 0$, the rank of $\sum_{k=1}^{3} d_k \mathbf{A}_k$ is also preserved. Moreover, including the parasitics makes the system more dissipative and shifts the corresponding eigenvalues further from zero. To verify that the proposed procedure is numerically robust in the considered operating range, the condition number has been calculated and plotted in Fig. 2, where it is shown to increase for very high values of r_{load} and d_1. However, it remains well below two orders of magnitude for the considered operating range, which does not represent a numerical problem for the IEEE double-precision floating-point machine arithmetics with precision on the order of 10^{-16} [54] (ANSI/IEEE Standard 754–1985).

The final numerical functions for m_1 and d_2 are plotted in Figs. 3 and 4, respectively. Since the capacitor voltage is continuous, the m_2 entry is about 1 and is not plotted here. As expected, the surfaces obtained are continuous and smooth. It can be noted in Fig. 3 that m_1 is 1 in the region corresponding

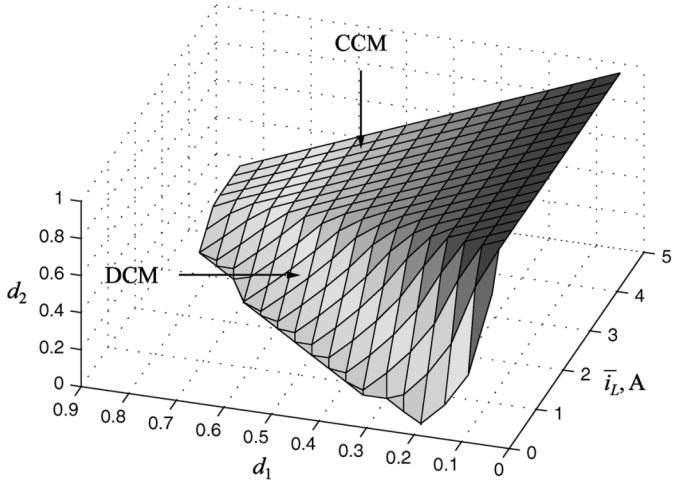

Fig. 4. Duty-ratio constraint d_2.

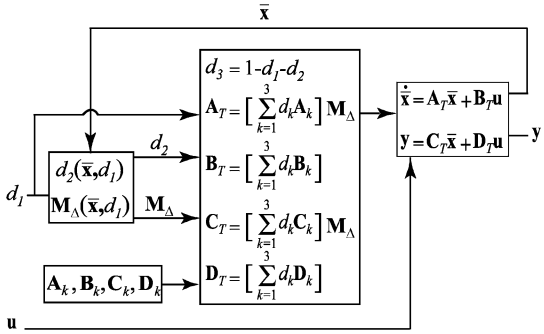

Fig. 5. Implementation of the proposed average-value model.

to CCM. In DCM, m_1 increases to compensate for the deficiency in conventional state-space averaging. In this mode, m_1 becomes a nonlinear function of d_1 and $\bar{i}_L$. In Fig. 4, d_2 has a flat surface corresponding to CCM, and varies linearly along the d_1 -axis independent of $\bar{i}_L$ (as expected, $d_2 = 1 - d_1$). In DCM, the surface of d_2 becomes non-linear and falls down.

Once the functions $d_2(d_1, \bar{i}_L)$ and $\mathbf{M}_\Delta(d_1, \bar{i}_L)$ are available and stored, the proposed average-value model is implemented according to the block diagram shown in Fig. 5. The system matrices for each subinterval are calculated numerically. For a given value of control variable d_1 and state vector $\bar{\mathbf{x}}$, the duty-ratio constraint and correction-term matrix are acquired through the lookup tables. Therefore, the computed total averaged system matrices dependent on state and duty cycle

$$\begin{cases} \mathbf{A}_T(\bar{\mathbf{x}}, d_1) = [d_1\mathbf{A}_1 + d_2\mathbf{A}_2 + d_3\mathbf{A}_3]\mathbf{M}_\Delta \\ \mathbf{B}_T(\bar{\mathbf{x}}, d_1) = [d_1\mathbf{B}_1 + d_2\mathbf{B}_2 + d_3\mathbf{B}_3] \\ \mathbf{C}_T(\bar{\mathbf{x}}, d_1) = [d_1\mathbf{C}_1 + d_2\mathbf{C}_2 + d_3\mathbf{C}_3]\mathbf{M}_\Delta \\ \mathbf{D}_T(\bar{\mathbf{x}}, d_1) = [d_1\mathbf{D}_1 + d_2\mathbf{D}_2 + d_3\mathbf{D}_3]. \end{cases} \tag{29}$$

These matrices are used to build a new continuous non-linear average-value model that replaces the discontinuous detailed model. Because the proposed model is not derived analytically but is instead constructed according to Fig. 5 with the duty-ratio constraint and correction matrix extracted numerically, it

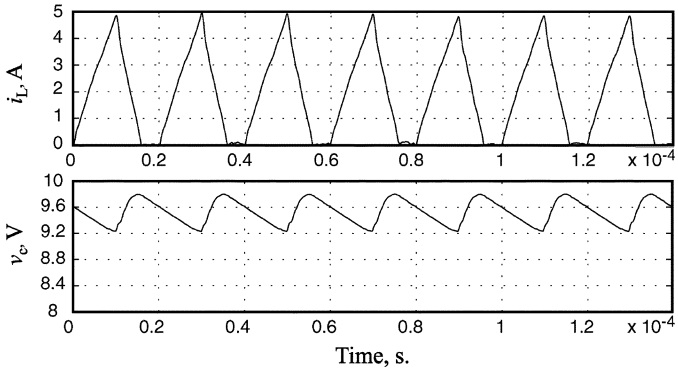

Fig. 6. Measured inductor current and capacitor voltage.

is herein referred to as the numerical average-value model (NAVM). The structure of the final model is

$$\begin{aligned}\dot{\bar{\mathbf{x}}} &= \mathbf{A}_T(\bar{\mathbf{x}}, d_1)\bar{\mathbf{x}} + \mathbf{B}_T(\bar{\mathbf{x}}, d_1)\mathbf{u} \\ &= \mathbf{f}(\bar{\mathbf{x}}, \mathbf{u}, d_1) \\ \mathbf{y} &= \mathbf{C}_T(\bar{\mathbf{x}}, d_1)\bar{\mathbf{x}} + \mathbf{D}_T(\bar{\mathbf{x}}, d_1)\mathbf{u} \\ &= \mathbf{g}(\bar{\mathbf{x}}, \mathbf{u}, d_1)\end{aligned} \tag{30}$$

which becomes available for large-signal transients as well as numerical linearization and subsequent small-signal frequency-domain analysis.

V. Case Studies

The boost converter described in the previous section is used as a benchmark in subsequent case studies. The detailed model is implemented in Matlab/Simulink [5] as a masked CMEX S-function using the toolbox [39]. The main parasitics of the hardware prototype have been included in the detailed model. The converter parameters summarized in the Appendix correspond to the hardware prototype that has been built. Since the proposed NAVM has been extracted from the detailed model, it only approaches the detailed model in terms of accuracy. The proposed model has been implemented and compared to the hardware prototype, the detailed model, and several previously published average-value models in both time and frequency domains.

A. Time Domain

The measured waveforms of the capacitor voltage and the inductor current corresponding to an operating point with $d_1 = 0.5$ and $r_{\text{Load}} = 15.12\ \Omega$ are shown in Fig. 6. It can be seen from this figure that parasitics cause nonlinearity of the current and voltage waveforms as compared to the idealized waveforms shown in Fig. 1(b). In an ideal boost converter, the steady-state average output voltage is always larger than or equal to the input voltage. However, if the parasitics are significant, the output voltage drops and can even fall below the input voltage due to poor switch utilization [55]. This phenomenon becomes especially pronounced when the duty cycle approaches unity. In large-signal average-value models, the effect of parasitics has

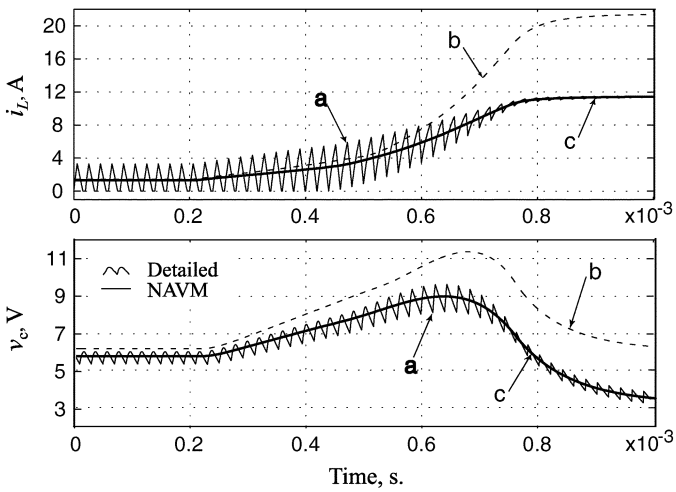

Fig. 7. Inductor current and capacitor voltage resulting from ramping-up the duty cycle: (a) detailed simulation, (b) corrected full-order model [28], and (c) proposed numerically constructed model (NAVM).

been included in models operating in CCM [26], [56] as well as DCM (full-order model [49], corrected full-order model [28]). However, not all types of parasitics are easy to include in all of the models. In particular, the averaged-switch model [28] can readily include the ESR of the inductor and capacitor, but the conduction losses due to the switching elements are neglected.

To demonstrate the effect of the transistor's on-state ESR, the following study is considered. The system initially operates in a steady-state with $r_{\text{Load}} = 7\ \Omega$ and $d_1 = 0.3$. At time $t = 0.0002$ s, the duty cycle d_1 increases as a linear ramp from 0.3 to 0.96, which is reached at $t = 0.00075$ s. As seen in Fig. 7, the converter mode changes from discontinuous to continuous, and finally the overloaded region of operation is reached (a—solid line). The model [28] was chosen because it automatically works in DCM and CCM. On the one hand, the results predicted by the model [28] (b—dashed line) certainly over estimate the final steady-state as well as the peak values for current and voltage. This study shows the importance of including the switch's parasitics. On the other hand, the responses predicted by the proposed NAVM (c—thick solid line) remain in excellent agreement with the transient produced by the detailed simulation throughout the entire study. Although it might be possible to re-derive the model [28] to include the transistor's parasitics, one of the advantages of the proposed model is that essentially any parasitics included in the detailed model become automatically included without additional effort.

The accuracy of the proposed model in predicting large-signal behavior in time-domain has also been verified by studying the effect of sudden changes in load. In the following study, the output of the boost converter was regulated using a proportional-plus-integral (PI) controller as shown on a simplified diagram in Fig. 8. The PI controller was designed to regulate the output voltage at 15 V by adjusting the duty cycle d_1. The controller parameters are $K_p = 0.1$ and $K_i = 50$. In the study being considered, the converter initially operates in a steady-state with a 40-Ω resistor attached to the output terminals. At $t = 0.0002$ s, the load is first changed to 80 sΩ. At $t = 0.0012$ s, another

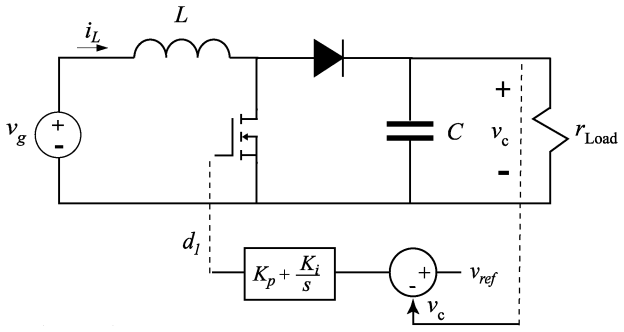

Fig. 8. Regulated boost converter.

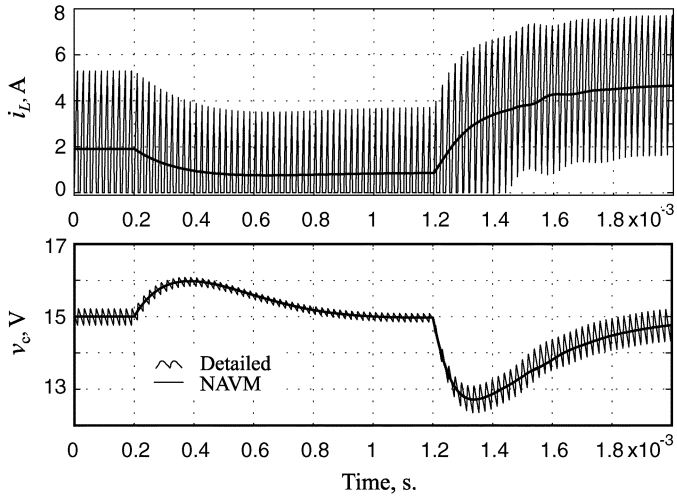

Fig. 9. Inductor current and capacitor voltage response to step changes in load.

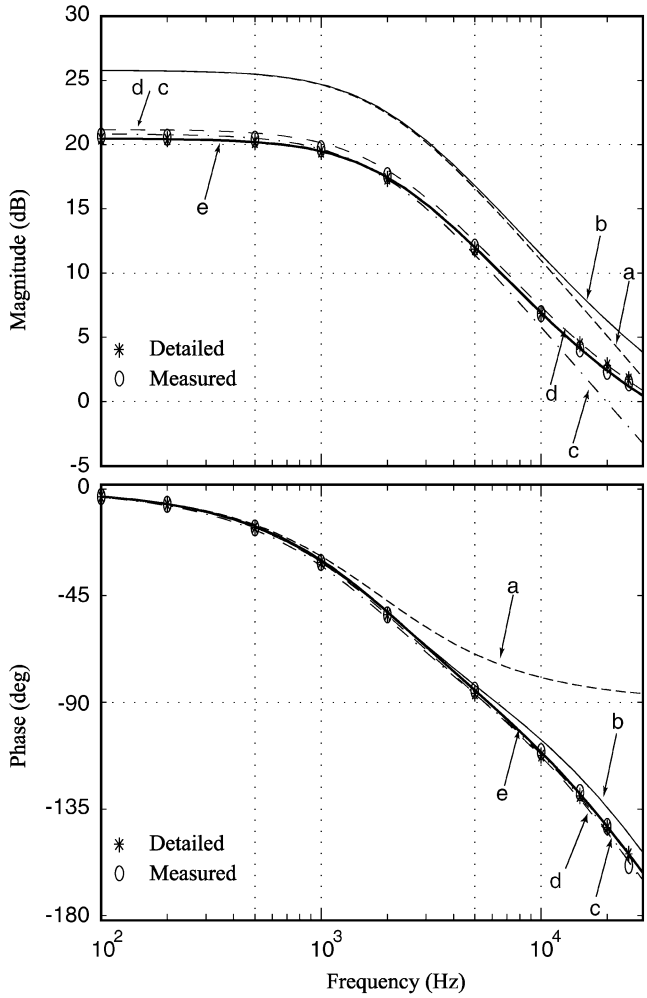

Fig. 10. Control-to-output transfer-function magnitude and phase: (a) reduced-order model (state-space averaging [32], circuit averaging [16]), (b) corrected full-order model without parasitics (state-space averaging [31], circuit averaging [28]), (c) full-order model with parasitics included (state-space averaging [33], circuit averaging [17] and [49]), (d) corrected full-order model with parasitics included (state-space averaging [31], circuit averaging [28] and [48]), and (e) proposed numerically constructed model (NAVM).

27 Ω resistor is connected in parallel to the load. The resulting time-domain transient is depicted in Fig. 9. As seen in Fig. 9, after the first change in load the converter still operates in DCM, whereas after the second change the converter mode changes to CCM. In each case, the control action is directed to bring the output voltage to the desired 15-V level. Throughout all transients, the large-signal behavior of the detailed model is accurately predicted by the proposed NAVM.

B. Frequency Domain

The control-to-output transfer-function is often considered in the literature for verifying the small-signal behavior of the converter models. The small signal-injection and subsequent frequency sweep method has been implemented to extract the small-signal transfer-function from the hardware prototype and from the detailed simulation corresponding to an operating condition defined by $r_{\mathrm{Load}} = 15.12\ \Omega$ and $d_1 = 0.5$. Using this method, the respective input and output variables were captured for each frequency point and processed using the FFT utility to extract the necessary magnitude and phase information. The measured inductor current and capacitor voltage for this operating point are shown in Fig. 6. The magnitude and phase of the corresponding control-to-output transfer-function are plotted in Fig. 10, where the (o) and (*) marks show the hardware measurement and detailed simulation at the same frequency points, respectively. As expected, the detailed simulation matches the hardware prototype very accurately. The transfer-function is evaluated up to 25 kHz, which is one-half of the switching frequency (50 kHz). Closer to the switching frequency the results become distorted due to interaction between the injected perturbations and the converter switching. In general, considering frequencies close to and above the switching frequency has limited use for the average-value model since the basic assumptions of averaging are no longer valid. Since the NAVM only approaches the detailed simulation in terms of accuracy, the data points produced by the detailed model are considered here as a reference.

In addition to the proposed NAVM, several commonly cited large-signal averaged models (Table I) are considered here for comparison purposes. Since the average-value models are continuous, they have been linearized at the same operating point, and respective transfer-functions then have been extracted. The results are superimposed in Fig. 10 for better comparison. In particular, the reduced-order lossless model [16], [32], (a—dashed line) clearly portrays a first-order response that

significantly under estimates the phase. Also, because the parasitics were not included, this model overestimates the dc gain by as much as 6 dBs. Next, the corrected full-order model [31] without parasitics is considered (b—solid line). Although a significant improvement over the reduced-order model (a—dashed line) is noticed, the dc gain remains off as before. Taking into account the effect of parasitics in analytically derived average-value models is not a trivial task. In particular, the derivation of the duty-ratio constraint becomes case-dependent and laborious. Including parasitics in the full-order model [17], [33] provides a nearly exact match in dc and the low-frequency range (c—dash-dot line), whereas the magnitude in high-frequency falls a bit lower. This discrepancy is attributed to the misallocation of the high-frequency pole and zero predicted by these types of full-order models. For more details on this phenomenon, the reader will find an interesting discussion and survey of full-order models in [13] and [31]. To include the necessary parasitics, the corrected full-order model [31] was considered. In particular, the ESRs of the inductor and the transistor were considered in the state matrices as well as the derivation of the duty-ratio constraint d_2. The resulting model (d—dashed line) provides the closest match to the detailed simulation among all analytically derived models, yet is a bit off in lower frequency. However, as shown in Fig. 10 (e—thick solid line), the developed NAVM predicts the control-to-output transfer-function with excellent agreement between the detailed simulation and the measured data.

VI. Conclusion

In this paper, we have presented a general approach for generating the state-space average-value models of PWM dc-dc converters. The proposed method relies on a corrected state-space averaging formulation and has a well-defined structure. The presented methodology overcomes the complexity and challenges common to many previously developed models when the parasitics of circuit elements are considered. The proposed numerically constructed model can function seamlessly in both CCM and DCM.

It is shown that obtaining an accurate full-order average-value model requires extracting the duty-ratio constraint and the correction term. The functions of the duty-ratio constraint and correction term were obtained numerically by running the detailed simulation. Even though establishing the proper average-value model requires running the detailed simulation, once established, the resulting model is continuous and valid for large-signal time-domain transient studies as well as for linearization and subsequent small-signal characterization of the overall system over a wide range. The proposed model is verified in time-domain as well as frequency-domain against the hardware prototype, the detailed simulation, and several other models commonly cited in the literature. The numerical average-value modeling developed in this paper provides a convenient framework for systematically averaging the PWM dc-dc converters and raises new possibilities for future research in automated average-value modeling.

Appendix

Please note that $v_g = 4$ V, $L = 6.2$ μ H, $r_L = 0.176$ $\Omega, r_{\rm sw} = 0.17$ Ω (MOSFET, IRF520V), switching frequency $f_s = 50$ kHz, $V_d = 0.4$ V (diode 12TQ035 forward voltage drop), $C = 14.715$ μF, and $r_c = 30$ mΩ.

References

[1] L. Jinjun, F. Xiaogang, F. C. Lee, and D. Borojevich, "Stability margin monitoring for DC distributed power systems via perturbation approaches," *IEEE Trans. Power Electron.*, vol. 18, no. 6, pp. 1254–1261, Nov. 2003.

[2] S. D. Sudhoff, S. Pekarek, B. Kuhn, S. Glover, J. Sauer, and D. Delisle, "Naval combat survivability testbeds for investigation of issues in shipboard power electronics based power and propulsion systems," in *Proc. IEEE PES*, 2002, vol. 1, pp. 347–350.

[3] A. Kislovski, R. Redl, and N. Sokal, *Dynamic Analysis of Switching-Mode DC/DC Converters*. New York: Van Nostrand-Reinhold, Jul. 1991.

[4] *Advanced Continuous Simulation Language (ACSL)*, Reference Manual, Version 11, MGA Software, 1995.

[5] *Simulink: Dynamic System Simulation for Matlab*, Using Simulink Version 5, The MathWorks Inc., Natick, MA, 2003.

[6] P. T. Krein, J. Bentsman, R. M. Bass, and B. L. Lesieutre, "On the use of averaging for the analysis of power electronic systems," *IEEE Trans. Power Electron.*, vol. 5, no. 2, pp. 182–190, Apr. 1990.

[7] F. C. Lee, R. P. Iwens, Y. Yu, and J. E. Triner, "Generalized computer-aided discrete time-domain modeling and analysis of DC-DC converters," *IEEE Trans. Ind. Electron. Control Instrum.*, vol. IECI-26, no. 2, pp. 58–69, May 1979.

[8] D. J. Shortt and F. C. Lee, "Improved switching converter model using discrete and averaging techniques," *IEEE Trans. Aerosp. Electron. Syst.*, vol. AES-19, pp. 190–202, May 1983.

[9] ——, "Extension of the discrete-average models for converter power stages," *IEEE Trans. Aerosp. Electron. Syst.*, vol. AES-20, pp. 279–289, May 1984.

[10] F. Guinjoan, J. Calvente, A. Poveda, and L. Martinez, "Large-signal modeling and simulation of switching DC-DC converters," *IEEE Trans. Power Electron.*, vol. 12, no. 3, pp. 485–494, May 1997.

[11] D. Maksimovic, A. M. Stankovic, V. J. Thottuveil, and G. C. Verghese, "Modeling and simulation of power electronic converters," *Proc. IEEE*, vol. 89, no. 6, pp. 898–912, Jun. 2001.

[12] R. Tymerski, "On the efficiency of sampled data modeling of switched networks," in *Proc. IEEE Workshop Comput. Power Electron.*, 1996, pp. 14–17.

[13] D. Maksimovic, "Computer-aided small-signal analysis based on impulse response of DC/DC," *IEEE Trans. Power Electron.*, vol. 15, no. 6, pp. 1183–1191, Nov. 2000.

[14] G. W. Wester and R. D. Middlebrook, "Low-frequency characterization of switched DC-DC converters," *IEEE Trans. Aerosp. Electron. Syst.*, vol. AES-9, pp. 376–385, May 1973.

[15] V. Vorperian, "Simplified analysis of PWM converters using the model of PWM switches, Part I: Continuous conduction mode," *IEEE Trans. Aerosp. Electron. Syst.*, vol. AES-26, pp. 490–496, May 1990.

[16] R. Tymerski and V. Vorperian, "Generation, classification and analysis of switched-mode DC-to-DC converters by the use of switching cells," in *Proc. Int. Telecommun. Energy Conf.*, 1986, pp. 181–195.

[17] V. Vorperian, "Simplified analysis of PWM converters using model of PWM switch, Part II: Discontinuous conduction mode," *IEEE Trans. Aerosp. Electron. Syst.*, vol. 26, no. 3, pp. 497–505, May. 1990.

[18] V. Vorperian, R. Tymerski, and F. C. Lee, "Equivalent circuit models for resonant and PWM switches," *IEEE Trans. Power Electron.*, vol. PE-4, no. 2, pp. 205–214, Apr. 1989.

[19] R. Tymerski, V. Vorperian, F. C. Lee, and W. T. Baumann, "Nonlinear modeling of the PWM switch," *IEEE Trans. Power Electron.*, vol. 4, no. 2, pp. 225–233, Apr. 1989.

[20] S. R. Sanders and G. C. Verghese, "Synthesis of averaged circuit models for switched power converters," *IEEE Trans. Circuits Syst.*, vol. 38, no. 8, pp. 905–915, Aug. 1991.

[21] R. D. Middlebrook and S. Cuk, "A general unified approach to modeling switching converter power stages," in *Proc. IEEE Power Electron. Spec. Conf.*, 1976, pp. 18–35.

[22] R. W. Brockett and J. R. Wood, "Electrical networks containing controlled switches," in *Proc. IEEE Symp. Circuit Theory*, Apr. 1974, pp. 1–11.

[23] S. K. Mazumder, A. H. Nayfeh, and D. Boroyevich, "Theoretical and experimental investigation of the fast- and slow-scale instabilities of a DC-DC converter," *IEEE Trans. Power Electron.*, vol. 16, no. 2, pp. 201–216, Mar. 2001.
[24] C. T. Rim, G. B. Joung, and G. H. Cho, "Practical switch based state-space modeling of DC-DC converters with all parasitics," *IEEE Trans. Power Electron.*, vol. 6, no. 4, pp. 611–617, Oct. 1991.
[25] A. Reatti, "Steady-state analysis including parasitic components and switching losses of buck and boost dc-dc converters under any operating condition," *Int. J. Electron.*, vol. 77, pp. 679–702, 1994.
[26] D. Czarkowski and M. K. Kazimierczuk, "Energy-conversion approach to modeling PWM dc-dc converters," *IEEE Trans. Aerosp. Electron. Syst.*, vol. 29, no. 3, pp. 1059–1063, Jul. 1993.
[27] A. Reatti and M. K. Kazimierczuk, "Small-signal model of PWM converters for discontinuous conduction mode and its application for boost converter," *IEEE Trans. Circuits Syst. I*, vol. 50, no. 1, pp. 65–73, Jan. 2003.
[28] G. Nirguade, R. Tirumala, and N. Mohan, "A new, large-signal average model for single-switch DC–DC converters operating in both CCM and DCM," in *Proc. IEEE Power Electron. Spec. Conf.*, 2001, vol. 3, pp. 1736–1741.
[29] K. Schenk and S. Cuk, "Small signal analysis of converters with multiple discontinuous conduction modes," in *Proc. IEEE Power Electron. Spec. Conf.*, 1998, vol. 1, pp. 623–629.
[30] L. G. De Vicuna, F. Guinjoan, J. Majo, and L. Martinez, "Discontinuous conduction mode in the SEPIC converter," in *Proc. MELECON*, 1989, pp. 38–42.
[31] J. Sun, D. M. Mitchell, M. F. Greuel, P. T. Krein, and R. M. Bass, "Averaged modeling of PWM converters operating in discontinuous conduction mode," *IEEE Trans. Power Electron.*, vol. 16, no. 4, pp. 482–492, Jul. 2001.
[32] S. Cuk and R. D. Middlebrook, "A general unified approach to modeling switching DC-to-DC converters in discontinuous conduction mode," in *Proc. IEEE Power Electron. Spec. Conf.*, 1977, pp. 36–57.
[33] D. Maksimovic and S. Cuk, "A unified analysis of PWM converter in discontinuous mode," *IEEE Trans. Power Electron.*, vol. 6, no. 4, pp. 476–490, Jul. 1991.
[34] P. Pejovic and D. Maksimovic, "Determination of network state in switching power converters," in *Proc. IEEE Power Electron. Spec. Conf.*, 1995, vol. 2, pp. 816–822.
[35] J. G. Kassakian, M. F. Schecht, and G. C. Verghese, *Principles of Power Electronics*. New York: Addison-Wesley, Jun. 1992.
[36] L. O. Chua and P. M. Lin, *Computer-Aided Analysis of Electronic Circuit, Algorithms and Computational Technique*. Englewood Cliffs, NJ: Prentice-Hall, 1975.
[37] J. Jatskevich, O. Wasynczuk, E. A. Walters, and C. E. Lucas, "Continuous state-space modeling of switched electric networks," in *Proc. IEEE Int. Conf. Contr. Appl.*, 2000, pp. 902–907.
[38] J. Jatskevich and T. Aboul-Seoud, "Automated state-variable formulation for power electronic circuits and systems," in *Proc. IEEE Int. Symp. Circuits Syst. (ISCAS'04)*, 2004, vol. 5, pp. 952–955.
[39] *Automated State Model Generator(ASMG)*, Reference Manual, Version 2, PC Krause and Associates Inc., 2002 [Online]. Available: www.pcka.com
[40] *Piece-wise Linear Electrical Circuit Simulation for Simulink (PLECS)*, User's Manual, Version 1.1, Plexim, 2005 [Online]. Available: www.plexim.com
[41] *SimPowerSystems for use with Simulink*, User's Guide Version 4, Hydro-Quebec, TransEnergie Technologies, The Mathworks, Inc., 2005 [Online]. Available: www.mathworks.com
[42] J. Sun and H. Grotstollen, "Averaged modeling of switching power converters: Reformulation and theoretical basis," in *Proc. IEEE Power Electron. Spec. Conf.*, 1992, vol. 2, pp. 1166–1172.
[43] ——, "Symbolic analysis methods for averaged modeling of switching power converters," *IEEE Trans. Power Electron.*, vol. 12, no. 3, pp. 537–546, May 1997.
[44] R. W. Erickson and D. Maksimovic, *Fundamental of Power Electronics*, 2nd ed. Norwell, MA: Kluwer, 2001.
[45] J. Chen, R. W. Erickson, and D. Maksimovic, "Averaged switch modeling of boundary conduction mode dc-to-dc converters," in *Proc. IECON'01*, 2001, vol. 2, pp. 844–849.
[46] S. Ang and A. Oliva, *Power-Switching Converters*. New York: CRC Press, 2005.
[47] J. Sun, D. M. Mitchell, M. F. Greuel, P. T. Krein, and R. M. Bass, "Modeling of PWM converters in discontinuous conduction mode: A reexamination," in *Proc. IEEE Power Electron. Spec. Conf.*, 1998, vol. 1, pp. 615–622.
[48] J. Sun, "Unified averaged switch models for stability analysis of large distributed power systems," in *Proc. APEC*, 2000, vol. 1, pp. 249–255.
[49] G. Zhu, S. Luo, C. Iannello, and I. Batarseh, "Modeling of conduction losses in PWM converters operating in discontinuous conduction mode," in *Proc. ISCAS*, 2000, vol. 3, pp. 511–514.
[50] S. B. Yakoov, D. Wulich, and W. M. Policka, "Resolution of an averaging paradox in the analysis of switched-mode dc-dc converters," *IEEE Trans. Aerosp. Electron. Syst.*, vol. 30, no. 2, pp. 626–632, Apr. 1994.
[51] C. Jingquan, D. Maksimovic, and R. W. Erickson, "Buck-boost PWM converters having two independently controlled switches," in *Proc. IEEE Power Electron. Spec. Conf.*, 2001, vol. 2, pp. 736–741.
[52] N. Femia, G. Spagnuolo, and M. Vitelli, "Steady-state analysis of soft-switching converters," *IEEE Trans. Circuits Syst. I*, vol. 49, no. 7, pp. 939–954, Jul. 2002.
[53] S. R. Sanders, J. M. Noworolski, X. Z. Liu, and G. C. Verghese, "Generalized averaging method for power conversion circuits," *IEEE Trans. Power Electron.*, vol. 6, no. 2, pp. 251–259, Apr. 1991.
[54] W. Gautchi, *Numerical Analysis: An Introduction*. Boston, MA: Birkhauser, 1997.
[55] N. Mohan, T. M. Undeland, and W. P. Robbins, *Power Electronics, Converters, Applications, and Design*. New York: Wiley, 1995, ch. 7.
[56] W. M. Polivka, P. R. K. Chetty, and R. D. Middlebrook, "State-space average modeling of converters with parasitics and storage-time modulation," in *Proc. IEEE Power Electron. Spec. Conf.*, 1980, pp. 119–145.

Ali Davoudi (S'04) received the B.Sc degree from Sharif University of Technology, Tehran, Iran, in 2003, the M.A.Sc. degree from the University of British Columbia, Vancouver, BC, Canada, in 2005, and is currently pursuing the Ph.D. degree at the University of Illinois at Urbana-Champaign, Urbana.

His research interests include average-value modeling of switching converters, multi-rate simulation of power electronic and electromechanical systems, and numerical modeling of magnetic devices.

Juri Jatskevich (M'99) received the M.S.E.E. and Ph.D. degrees from Purdue University, West Lafayette IN, in 1997 and 1999, respectively.

He stayed at Purdue as a Post-Doctoral Research Associate and Research Scientist, as well as consulted for P. C. Krause and Associates, Inc. Since 2002, he has been an Assistant Professor of electrical and computer engineering at the University of British Columbia, Vancouver, BC, Canada. His research interests include electrical machines, power electronic systems, and simulations.

Tom De Rybel received the Industrial Engineer degree in electronics design from Hogeschool Gent, Gent, Belgium, in 2002 and the M.A.Sc. degree from he the University of British Columbia, Vancouver, BC, Canada in 2005 where he is currently pursuing the Ph.D. degree in power systems.

His research interests are power electronics, analog design, real-time simulation, high-voltage measurement systems, large-scale data acquisition synchronization, and biomedical modeling.